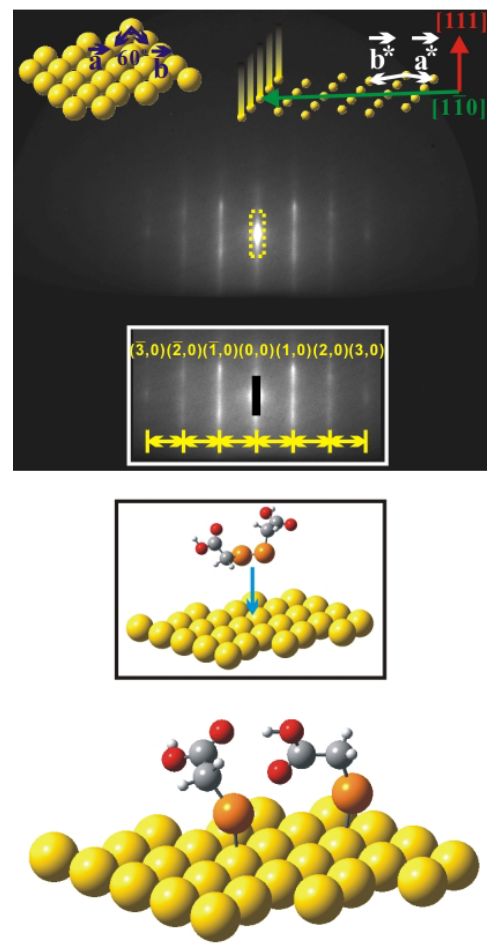


# Chapter 11

## Structures and Dynamics of Self-Assembled Surface Monolayers<sup>†</sup>



<sup>†</sup>adapted from C.-Y. Ruan, D.-S. Yang, A. H. Zewail, *J. Am. Chem. Soc.* **126**, 12797 (2004).

## Introduction

When a beam of ultrashort electron pulses impinges on a crystal surface, diffraction patterns can be resolved in time (femtosecond to picosecond) and in space (picometer). Because of the large cross section for electron interaction with matter, the sensitivity is sub-monolayer. The methodology of ultrafast electron crystallography (UEC) makes possible the study of surface atoms and adsorbates of nanometer length scale. In this chapter, I briefly describe our initial study of self-assembled (*1*) adsorbates on metal surfaces. Specifically, we studied single-crystal clean surfaces of Au(111) with and without a monolayer of reaction involving the assembly of 2-mercaptoacetic acid from 2,2'-dithiodiacetic acid (*2*). Monolayers of iron hemes were also studied. The current investigation is different from the studies of Langmuir–Blodgett films of fatty acids and phospholipids made in our group (*3, 4*) in terms of the nature of the surface assemblies and the interaction involved at the interface. With UEC, we are able to observe and isolate structural dynamics of the substrate (gold) and adsorbate(s) following an ultrafast temperature jump.

The single-crystal substrate has a long-range order, which results in well-defined Bragg diffraction spots and streaks in the Laue zones. In the presence of adsorbates, new diffraction features appear depending on the degree of order—Bragg spots if perfectly ordered and Debye–Scherrer rings if ordered (within small domains) but randomly oriented. Using the method of diffraction frame referencing (*5*), gating of the distinct coherent diffraction features (Bragg spots, streaks or Debye–Scherrer rings) or the incoherent features (diffuse background or Kikuchi scattering) as a function of time allows for independent isolation of dynamics originated from different structures. This isolation is aided by the ability to obtain the diffraction at small and large angles in real

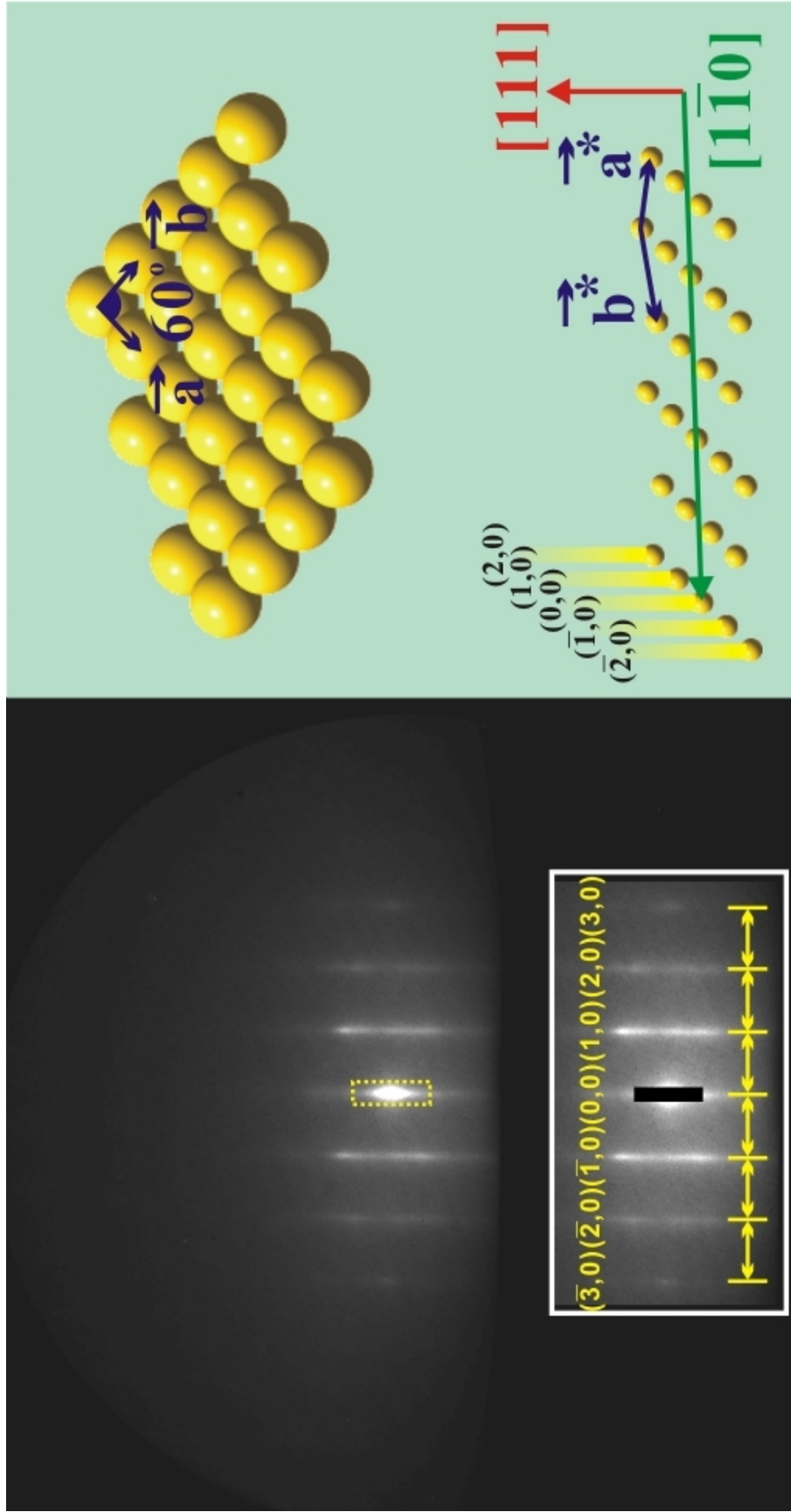


**Fig. 1.** (Left) Diffraction images of single-crystal Au(111). The inset shows the streaks at higher contrast, indexed according to the Miller indices  $(h, k)$ , where  $k$  represents the order of Laue zones. (Right) Real-space representation of Au(111) (top) together with reciprocal lattice rods corresponding to the two-dimensional Au(111) surface (bottom).

time. UEC is thus uniquely suited for examining structural dynamics at the interface with atomic-scale spatial and temporal resolutions.

### **Materials and Experimental Section**

Gold(111) films of 150 nm thickness on mica substrates were purchased from Molecular Imaging; the single-crystal domain from STM images is more than 200×200 nm. The thiolated surface was prepared following procedures of Ref. 2, which were also used for the preparation of thiolated alkanes and heme assembly. In solution, the disulfide bond of 2,2'-dithiodiacetic acid breaks to form the more stable sulfur–gold interfacial bonds (2, 6). The samples were then rinsed copiously with ethanol, dried in nitrogen ambient, and immediately mounted onto the goniometer of our UEC diffraction chamber (at a pressure of  $\sim 5 \times 10^{-10}$  Torr). To initiate the change, we used near-IR 800-nm femtosecond pulses, and to probe, we generated ultrashort electron pulses (30 keV). The pulses can be as short as 300–600 fs but here a pulse width of  $\sim 2$  ps was used at the number of electrons per pulse applied. The electron pulses were timed to arrive either before or after the initiating pulse, and diffraction patterns were recorded on a CCD camera assembly. All experiments were performed at room temperature except for studies of diffuse scattering at small angles when the substrate temperature was reduced to 120 K to suppress thermal background.

### **Results and Analysis**

For the clean unmodified gold substrate, the diffraction patterns consist of well-resolved Bragg spots and streak features (Fig. 1). The positions of these spots and streaks, together with the geometrically established specular reflection and shadow edges

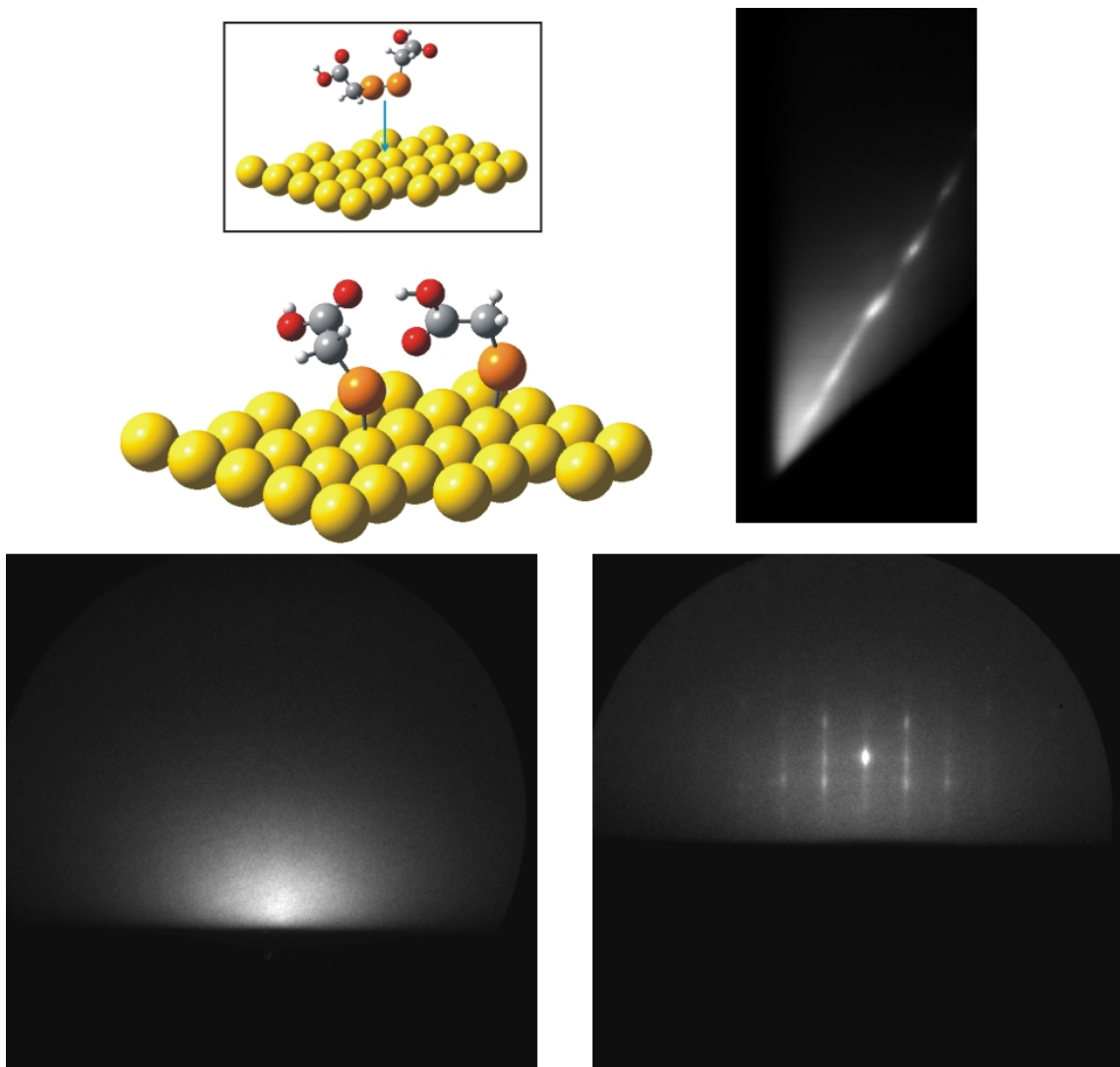


**Fig. 2.** (Top left) Representation of the structures involved in the reaction of 2,2'-dithiodiacetic acid and a clean gold surface. (Top right) The experimentally observed rocking curve  $s$  (vertical) vs  $\theta_{in}$  (horizontal), where  $s$  is the scattering vector and  $\theta_{in}$  is the incidence angle. Note the different orders observed as a function of  $\theta_{in}$ , which were detected by gating the (0,0) streak. (Bottom left) Static diffuse scattering obtained without temporal resolution at a small incidence angle of  $\sim 1^\circ$ . (Bottom right) Gold-type streaks (see Fig. 1) obtained for the thiolated surface when the incidence angle is relatively large ( $\sim 4.2^\circ$ ). Note that the shadow edge is different for small- and large-angle diffractions, reflecting the geometry of electron incidence on the surface.

for calibration, directly provide the structure of the two-dimensional reciprocal lattice of the (111) planes of the face-centered-cubic crystal. As noted in Fig. 1, we observed the streaks in the zeroth-order Laue zone, indexed by  $(h, 0)$ , where the integer  $h$  is a Miller index. The rods of the two-dimensional reciprocal lattice are modulated because of the few surface layers in the  $c^*$  direction of the reciprocal space. From their horizontal separation in the diffraction pattern, the lattice spacing of the Au(111) plane was obtained, which is consistent with that of the literature x-ray value ( $d_{\text{Au-Au}} = 2.884 \text{ \AA}$ ). We also obtained the rocking curves and observed the different orders satisfying the Bragg/Laue conditions:  $s \cdot d_{(111)} = 2\pi n$ , where  $n$  is the order of diffraction and  $s$  is the scattering vector,  $s = (4\pi/\lambda_e)\sin(\theta/2)$ , with  $\theta$  being the acute deflection angle between the incident and outgoing wave vectors and  $\lambda_e$  the wavelength of the electron (at 30 keV,  $\lambda_e \approx 0.07 \text{ \AA}$ ). From the rocking curves, the  $(c^*)$  interplanar Bragg reflections for clean and thiolated gold surfaces were identified at incidence angles of  $3.4$  and  $4.2^\circ$ , and these Bragg spots were gated to give lattice dynamics of the (111) planes at  $d_{(111)} = 2.355 \text{ \AA}$ .

The self-assembled monolayer (SAM) on gold results in a much different diffraction pattern, depending on the angle of incidence (Fig. 2). At low incidence angles ( $\sim 1^\circ$ ), diffuse scattering was observed (Fig. 2, bottom left), while at relatively higher incidence angles ( $\sim 4.2^\circ$ ), the gold-type behavior of Fig. 1 was basically recovered (Fig. 2, bottom right). Accordingly, the SAM reaction shown in Fig. 2 for 2-mercaptopropionic acid on gold resulted in surface diffraction of what appears to be a randomly oriented adsorbate; however, when the electron was allowed (at the larger incidence angles) to penetrate the bulk surface layers, gold diffraction was seen even with the thiolated surface layer being present. To check for the order of diffraction we compared rocking curves with and without thiolation (Fig. 2, top right). This *static* picture was completely

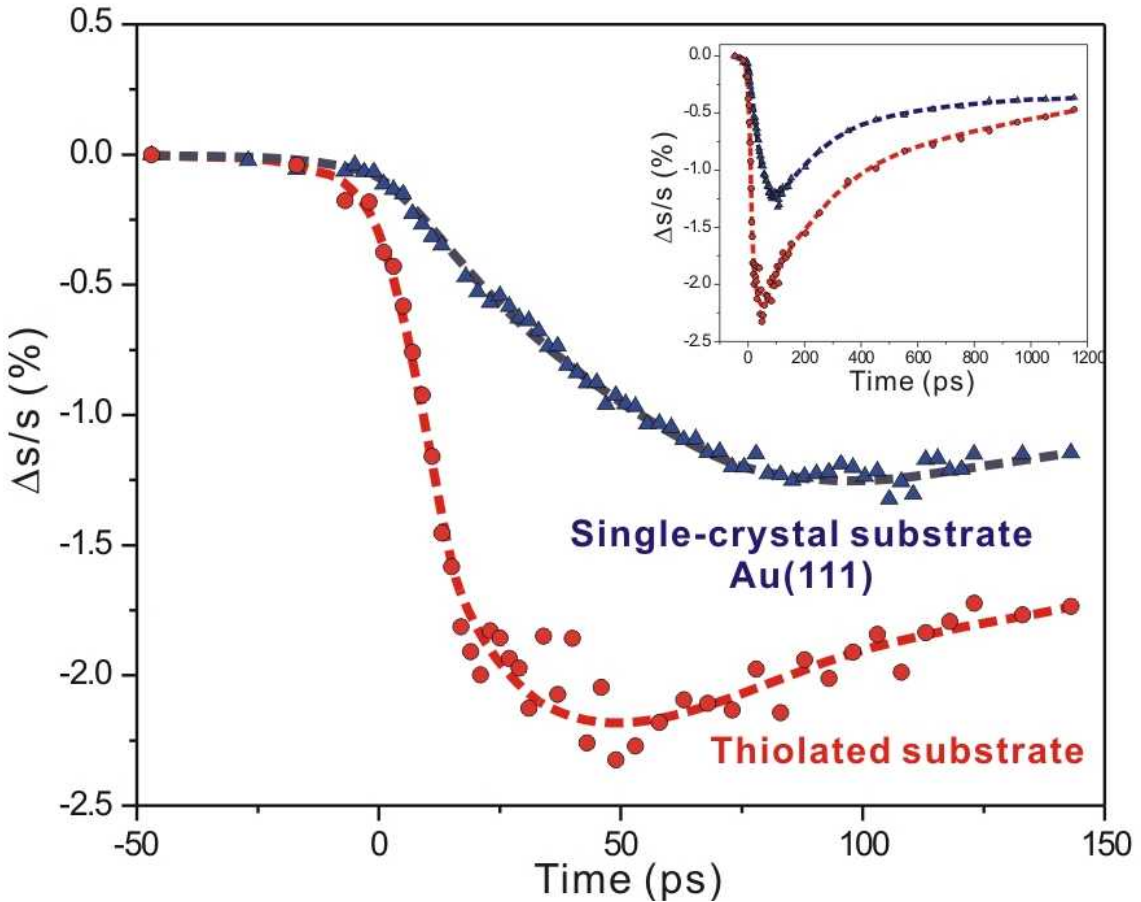
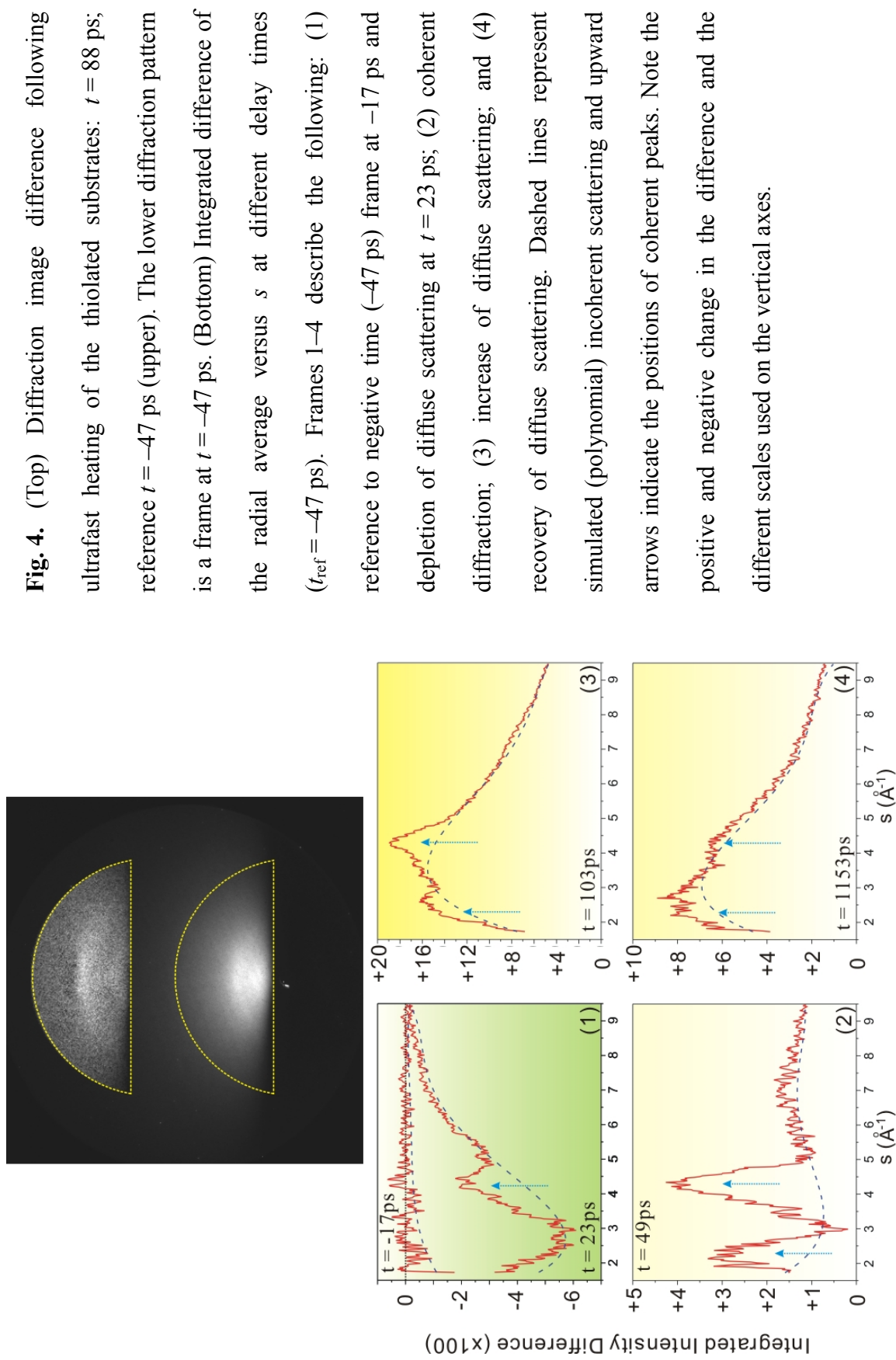


**Fig. 3.** Relative changes of the scattering vector  $s$  vs time for the Bragg spot monitored. The inset shows the restructuring on a longer time scale. The dashed lines are guides to the eye.

altered when the dynamics was obtained using ultrafast initiation by a heating pulse.

Following the ultrafast temperature jump, the structural evolution from Bragg spots was monitored: peak position (lattice expansion), width (homogeneity of the long-range order), and intensity (atomic motions). Clean and thiolated surfaces show striking differences in structural dynamics (Fig. 3). As manifested in the shift of the Bragg spot position in the diffraction pattern, the thiolated surface needs only  $\sim 20$  ps to reach 80% of its maximum change. This change corresponds to a lattice expansion of 2.2%, or  $52$  mÅ increase in the (111) interplanar distance. For the clean gold surface,



however, it requires at least  $\sim 55$  ps to reach 80%, depending on cleanliness, of its maximum change (1.3%). The determined surface movement on the order of 0.1 Å is the precursor impulse for adsorbate and bulk lattice heating.

It has been found that the degree of cleanliness and/or surface reconstruction changes the time response; e.g., freshly prepared gold samples give an even slower response. However, the distinct difference between unthiolated and thiolated surfaces is reproducible. It should be noted that the substrate–adsorbate composite fully recovers within 1 ms according to our instrumental repetition rate, as the surface is observed to restructure back to the same ground state (Fig. 3, inset); there is no influence of the probing electrons on the surface, as no irreversible loss of structure (deterioration of the diffraction pattern) was seen. Temporal evolution of the vertical width of the Bragg spot, which reflects the long-range order of the stacked (111) planes, is also noticeable: the thiolated surface shows initial broadening (loss of order) followed by narrowing of the peak (enhancement of order), while the clean gold surface shows a slower response. The decrease in peak intensity reflects change in the atomic motion and temperature, and again for the thiolated surface, the behavior is different from that of clean gold. It is noted that for a clean gold film, the temporal profiles for the position, vertical width and intensity of the Bragg spot are similar.

At an incidence angle of  $\sim 1^\circ$ , i.e., gating the molecular diffraction region, we observed the emergence of Debye–Scherrer rings and the dramatic change in the diffraction background, but only after the IR laser heating (Fig. 4). In the radially averaged one-dimensional diffraction intensity curves, these changes in structural dynamics of the adsorbates were followed by monitoring the evolution of diffraction peaks and background. The near maximum formation of the long-range order is reached

at 49 ps, as observed in the prominence of the coherent diffraction peaks (Fig. 4, bottom). For the incoherent scattering background, an ultrafast increase of intensity ( $\sim 5$  ps) just after the laser heating is noted and followed by a depletion of intensity for  $\sim 30$  ps; at longer times the background continues to increase (Fig. 4, bottom). Remarkably, these difference frames are showing the *depletion* (negative difference) at early times and simultaneously the appearance of a coherent ring structure, while at longer times the diffuse signal is positively *increasing* at the expense of the coherent signal. The restructuring is not complete even at  $t > 1$  ns. As noted in the inset of Fig. 3, at  $t \sim 1$  ns there still remains expansion of the lattice, and similarly here the adsorbate has not fully relaxed and mostly disordered. Ultimately, the frame difference of  $-17$  ps would be recovered, as evidenced from the decrease in scattering amplitude between the frames at long times; see, e.g.,  $t = 103$  and  $1153$  ps (Fig. 4).

## Discussion

These observations are rich for deciphering structural dynamics of the substrate and adsorbate. First, the observed lattice dynamics of clean gold substrate is unexpected. Although electron–phonon coupling is known in metallic gold to occur within  $\sim 1$  ps (7, 8), the observed increase in lattice expansion in nearly 50 ps (instead of a decrease after  $\sim 1$  ps) elucidates the existence of a nonequilibrium state among the modes responsible for surface and lattice expansion. Since our electron probing region is within the optically heated depth [ $\sim 13$  nm; the skin depth equals to  $\lambda/4\pi k$ , with the imaginary part of refractive index  $k$  being  $\sim 5$  at  $\lambda = 800$  nm (9)], complete equilibration would not lead to the observation of further expansion after 1 ps.

Consistent observations have been made by Maznev *et al.* using the time-resolved

probe-beam deflection technique (10): They found similar slow surface expansion of supported gold films on the order of 100 ps and dependent on the film thickness, and these results showed that the long surface expansion rise time is due to the fast nonequilibrium electron diffusion into the bulk and the slow, accumulated expansion at the surface with the longitudinal sound velocity of 3240 m/s (10). It is noted that our observed dynamics may also have contribution from the slower coupling between high-frequency (local) modes excited at an early time and the lattice acoustic (coherent and long-range) modes that lead to the expansion; at longer times the system equilibrates and the lattice restructures, as shown in Fig. 3. Because of the mismatch between mode frequencies, this behavior is reminiscent of energy redistribution in molecules (11), and the time constant is not significantly different from those of semiconductors (see Chs. 4 and 5).

The change in expansion dynamics from the unmodified gold surface to the thiolated surface is thus consistent with the adsorbate having many modes. The surface assembly provides another direction for the energy flow instead of the unidirectional diffusion into the bulk. In addition, excess energy can couple more effectively to the vibrational modes of the adsorbate molecules than to the mismatched low-frequency acoustic modes of bulk lattice, which practically retains more energy near the surface region (leading to a larger surface expansion) and reduces the expansion rise time, as shown in Fig. 3.

The diffraction pattern at small angle and negative time, i.e., when the electron pulse diffracts before the arrival of the heating pulse, appears to be diffuse. However, as shown in Fig. 4, the coherent scattering (Debye–Scherrer rings) becomes dominant at a positive time of  $t = 49$  ps. Thus, the timing of the electron pulse is critical for structural

isolation and determination. Because the  $s$  value below the shadow edge is  $\leq 1.5 \text{ \AA}^{-1}$  at our incidence angle, the coherent peak positions are of  $n = 2$  and 3. From the corresponding  $s$  values we obtained a lattice constant of  $5 \pm 0.6 \text{ \AA}$  for the molecular assembly. This distance is reasonable given that typical S–S distance on a gold(111) surface is  $\sim\sqrt{3}$  times the Au–Au distance ( $2.884 \text{ \AA}$ ), i.e.,  $\sim 5 \text{ \AA}$  (12).

Dynamically speaking, this temporally isolated coherent diffraction from the assembly reaches its maximum but then is lost to the incoherent background at longer times, indicating that the orientational order of the assembly is dynamically controlled, and we can establish the time scale for this “ultrafast annealing.” The evolution of background scattering also reflects the change in the long-range surface order and homogeneity. The initial temperature jump introduces dramatic depletion of the background within the first  $\sim 30 \text{ ps}$ , and then a swift inversion of the trend appears, during which the molecular coherent peak sharpens and the background scattering begins to increase significantly. The initial depletion reflects the transient temperature-induced homogeneity, while after  $30 \text{ ps}$  the identity of inhomogeneous surface distributions leads to the increase of the background intensity (Fig. 4). Clearly, the time resolution is essential for isolating coherent structural dynamics of the self-assembled layers, which statistically are not ordered at long times.

## Concluding Remarks

This study has demonstrated that the structure and dynamics of self-assembled monolayer and metal substrate can be isolated and studied with atomic-scale spatial and temporal resolutions and with monolayer sensitivity. This is made possible using UEC and its ability to isolate diffraction at different angles of real-time frames with

atomic-scale resolution. Moreover, it is shown that for complex molecular structures, the resolution in time is crucial for observing the coherent diffraction (ordered structure), otherwise buried in diffuse scattering (disordered structure), and at long times disorder of assembly is evident. With this in mind, we also studied monolayers of alkanethiols and thio-derivatized hemes on Au(111) surfaces, and were able to record the diffractions and their changes with time although the patterns are diffuse. Intriguingly, horizontal (asymmetric) intensity redistribution in the diffuse scattering was seen from heme samples at positive times, which, on the basis of the annealing phenomenon described previously, can be attributed to the transient reorganization of the sulfur–gold bonds at the interface and rotation of the heme groups, causing changes in the efficiency of electron scattering in the horizontal direction. In the future, the applications of UEC to SAMs of other biological networks may reveal other structural and dynamical information of interest.

### References:

1. C. D. Bain, G. M. Whitesides, *Science* **240**, 62 (1988) and cited references therein.
2. M. Shimizu *et al.*, *Biochem. Biophys. Res. Commun.* **310**, 606 (2003) and cited references therein.
3. M. T. Seidel, S. Chen, A. H. Zewail, *J. Phys. Chem. C* **111**, 4920 (2007).
4. S. Chen, Ph.D. thesis, California Institute of Technology (2007).
5. R. Srinivasan, V. A. Lobastov, C. Y. Ruan, A. H. Zewail, *Helv. Chim. Acta* **86**, 1763 (2003).
6. R. G. Nuzzo, D. L. Allara, *J. Am. Chem. Soc.* **105**, 4481 (1983).
7. C. K. Sun, F. Vallée, L. H. Acioli, E. P. Ippen, J. G. Fujimoto, *Phys. Rev. B* **50**,

- 15337 (1994) and cited references therein.
8. C. Suárez, W. E. Bron, T. Juhasz, *Phys. Rev. Lett.* **75**, 4536 (1995) and cited references therein.
  9. P. B. Johnson, R. W. Christy, *Phys. Rev. B* **6**, 4370 (1972).
  10. A. A. Maznev, J. Hohlfeld, J. Gütde, *J. Appl. Phys.* **82**, 5082 (1997) and cited references therein.
  11. P. M. Felker, A. H. Zewail, *Phys. Rev. Lett.* **53**, 501 (1984).
  12. A. Ulman, *Chem. Rev.* **96**, 1533 (1996).